Published in "Proceedings of the National Academy of Sciences 116(16): 7766–7771, 2019"
which should be cited to refer to this work.

Diffusing wave microrheology of highly scattering concentrated monodisperse emulsions

Ha Seong Kim[a], Nesrin Şenbil[b], Chi Zhang[b], Frank Scheffold[b,1], and Thomas G. Mason[a,c,1]

[a]Department of Chemistry and Biochemistry, University of California, Los Angeles, CA 90095; [b]Department of Physics, University of Fribourg, CH-1700 Fribourg, Switzerland; and [c]Department of Physics and Astronomy, University of California, Los Angeles, CA 90095

Edited by Steve Granick, IBS Center for Soft and Living Matter, Ulju-gun, Ulsan, Republic of Korea, and approved February 27, 2019 (received for review October 3, 2018)

Motivated by improvements in diffusing wave spectroscopy (DWS) for nonergodic, highly optically scattering soft matter and by cursory treatment of collective scattering effects in prior DWS microrheology experiments, we investigate the low-frequency plateau elastic shear moduli G'_p of concentrated, monodisperse, disordered oil-in-water emulsions as droplets jam. In such experiments, the droplets play dual roles both as optical probes and as the jammed objects that impart shear elasticity. Here, we demonstrate that collective scattering significantly affects DWS mean-square displacements (MSDs) in dense colloidal emulsions. By measuring and analyzing the scattering mean free path as a function of droplet volume fraction ϕ, we obtain a ϕ-dependent average structure factor. We use this to correct DWS MSDs by up to a factor of 4 and then calculate G'_p predicted by the generalized Stokes–Einstein relation. We show that DWS-microrheological $G'_p(\phi)$ agrees well with mechanically measured $G'_p(\phi)$ over about three orders of magnitude when droplets are jammed but only weakly deformed. Moreover, both of these measurements are consistent with predictions of an entropic–electrostatic–interfacial (EEI) model, based on quasi-equilibrium free-energy minimization of disordered, screened-charge–stabilized, deformable droplets, which accurately describes prior mechanical measurements of $G'_p(\phi)$ made on similar disordered monodisperse emulsions over a wide range of droplet radii and ϕ. This very good quantitative agreement between DWS microrheology, mechanical rheometry, and the EEI model provides a comprehensive and self-consistent view of weakly jammed emulsions. Extensions of this approach may improve DWS microrheology on other systems of dense, jammed colloids that are highly scattering.

microrheology | jamming | emulsions | diffusing wave spectroscopy | viscoelasticity

Diffusing wave spectroscopy (DWS) (1, 2) is a dynamic light-scattering (DLS) technique that can be used to measure time-dependent mean-square displacements (MSDs), $\langle \Delta \boldsymbol{r}^2(t) \rangle$, of uniform spherical probe particles in opaque, highly scattering colloidal dispersions. In DWS, the transport of light is modeled as a random walk having an optical transport mean free path ℓ^*. The diffusion equation is then applied to a specific sample-cell geometry, which typically has a thickness far in excess of ℓ^*, while taking into account the illumination and detection configuration used. DWS is a powerful approach because it is capable of measuring colloidal dynamics over a wide range of time scales, and it is also sensitive to very small probe displacements approaching 1 Å (1–5). Provided that the scattering probes are well dispersed and dilute, their self-motion MSDs can be accurately inferred from the measured DWS intensity autocorrelation function (1–5).

By contrast, for probes at densities well beyond the dilute limit, collective light-scattering effects could significantly influence decays and plateaus in DWS correlation functions, particularly when probes are at high-volume fractions ϕ and have diameters comparable to or smaller than the wavelength of the illuminating light (4). Because the standard analytical framework of DWS neglects collective scattering of colloidal probes at high densities, DWS MSDs extracted for such dense colloidal systems do not necessarily represent the true self-motion of the probes. Consequently, using DWS MSDs for thermal-entropic passive microrheology (6, 7) of dense dispersions, including concentrated emulsions, would likely lead to inaccurate predictions of their linear viscoelastic moduli, since passive microrheology requires accurate self-motion MSDs in the generalized Stokes–Einstein relation (GSER) (6, 8).

Despite these potential issues related to collective scattering, DWS MSDs have been used since the inception of passive microrheology to infer the linear viscoelastic response of numerous soft materials, such as hard spheres (6, 8), emulsions (6, 8), polymer solutions (6, 9–11), DNA solutions (12–14), actin solutions (15–17), microgels (18), and micellar solutions (19–21). For at least some of these systems, and particularly for concentrated emulsions, collective scattering could play a significant role. In addition, early DWS studies of nonergodic soft materials (8), including concentrated emulsions, were taken using a simple DWS apparatus that did not force a final long-time decay (22). As a consequence, for such nonergodic materials, the values of the plateaus varied significantly from run to run, precluding accurate comparisons of shear elastic

Significance

By treating collective light scattering in dense colloidal systems, we improve the analysis approach for diffusing wave spectroscopy (DWS), a dynamic light-scattering technique developed for white, highly scattering soft materials. Using this improved DWS analysis, we accurately measure the bounded translational motion of crowded oil droplets within concentrated monodisperse oil-in-water emulsions resembling mayonnaise. We show that the plateau elastic shear moduli of such emulsions determined by passive microrheology, based on this true bounded droplet motion and the generalized Stokes–Einstein relation, match very closely with mechanical measurements and model predictions as the droplets become more tightly jammed. This excellent quantitative agreement represents a major improvement over prior microrheology measurements on similar jammed emulsions that yielded only qualitative trends.

Author contributions: F.S. and T.G.M. designed research; H.S.K., N.S., and C.Z. performed research; H.S.K., N.S., C.Z., F.S., and T.G.M. analyzed data; and H.S.K., F.S., and T.G.M. wrote the paper.

Conflict of interest statement: F.S. is a board member and shareholder of LS Instruments AG.

[1]To whom correspondence may be addressed. Email: mason@physics.ucla.edu or frank.scheffold@unifr.ch.

This article contains supporting information

moduli obtained using DWS-GSER microrheology with mechanical rheometry (8).

To alleviate this undesirable variability in DWS correlation functions of nonergodic materials, one effective solution involves introducing a second cell (23, 24) or a slowly moving rigid scatterer (25, 26) (e.g., etched glass having a rough surface) into the light path that includes the nonergodic soft material. The motion of this additional moving scatterer forces the DWS correlation function to decay fully at a certain long time, which can be controlled by the rate of its motion, without significantly affecting the correlation function at earlier times. This improvement in technique effectively ensures that early-time behavior and plateau values of the DWS correlation function, obtained by the digital correlator's hardware and software, are reproducible from run to run both for ergodic and for nonergodic soft materials, at least over time scales significantly shorter than those associated with the time scale of the final forced decay (24–26). Moreover, if the slowly moving rigid scatterer is rotated at a fixed angular frequency, such that identical scatterers of this rigid object move into the illuminating beam periodically every cycle, then DWS echo signals (27) can also be collected at times longer than the forced decay. Such DWS echo signals are useful because they extend the temporal range of the DWS correlation function and extracted MSDs to time scales of tens of seconds while keeping the total measurement time short, on the order of minutes.

Motivated by these improvements in DWS techniques for nonergodic systems and also by the need to rectify collective scattering effects in DWS of dense colloidal systems, which can adversely affect passive microrheology, we present a systematic experimental comparison of the plateau elastic shear moduli, G'_p, measured using both mechanical rheometry and modern DWS microrheology, of disordered, jammed, microscale monodisperse emulsions, as a function of ϕ. Because uncertainties in G'_p can be large in the jamming regime even for small uncertainties in ϕ, we perform both DWS and mechanical rheometry experiments on exactly the same emulsion samples, each of which has a highly controlled ϕ. By using a high-viscosity oil inside our droplets, we suppress entropic interfacial fluctuations that can otherwise be detected by DWS at very early times for less viscous droplets (28), and, to avoid complications introduced by inertia, we focus on time scales longer than inertial time scales (3, 6) when making microrheological interpretations. Here, we show that long-time plateau MSDs measured using DWS, when corrected for the ϕ-dependent average structure factor and used in the GSER, yield $G'_p(\phi)$ which matches that of macroscopic mechanical rheometry, as well as an analytical model of droplet jamming, over about three orders of magnitude as droplets jam. Our study represents a major improvement over earlier microrheological measurements made using a simpler and less refined DWS technique (6, 8) that was not as accurate, did not account for the ϕ-dependent average structure factor, and demonstrated only a qualitative trend in $G'_p(\phi)$ in the jamming regime compared with mechanical rheometry. Moreover, our study goes beyond recent light-scattering work on concentrated nanoemulsions that did not include a direct comparison with a measured $G'_p(\phi)$ and that used an ad hoc ϕ-independent correction factor to rescale the microrheological $G'_p(\phi)$ (29). Given the strikingly accurate quantitative comparison that we have obtained for jammed emulsions, we anticipate that our experimental and analytical approaches could serve as a basis for improving quantitative DWS-GSER passive microrheology of other jammed disordered systems of highly scattering colloidal objects.

Results and Discussion

Mechanical Plateau Shear Modulus and Entropic–Electrostatic–Interfacial Model. In Fig. 1*A*, we compare the mechanically measured plateau elastic shear moduli $G'_{p,mech}$ of the monodisperse emulsion in this study, which has an average droplet radius a = 459 nm (*Materials and Methods*), to predicted values of $G'_{p,EEI}$ obtained by the entropic–electrostatic–interfacial (EEI) model (30) for concentrated, ionically stabilized, disordered monodisperse oil-in-water (O/W) emulsions near and above the jamming point. The EEI model assumes that minimization of a quasi-equilibrium free energy, which includes terms related to entropic crowding, screened electrostatic repulsions, and droplet interfacial deformation, is a reasonable approximation for disordered emulsions in the weak jamming limit. The parameter values that we use here in the EEI model are those that have been shown to describe the mechanically measured $G'_{p,mech}(\phi)$ of other similar polydimethyl siloxane (PDMS) O/W monodisperse emulsions having nano- and microscale radii at the same 10-mM bulk SDS concentration (30). By determining the dominant contribution to $G'_{p,EEI}$ at different ϕ (30), we find that $0.562 < \phi < 0.592$ corresponds to the electrostatically jammed regime (i.e., screened charge repulsion dominates) and $\phi \geq 0.592$ corresponds to the interfacially jammed regime (i.e., droplet interfacial deformation dominates). The entropic regime lies below the ϕ range that we have explored here. We find that $G'_{p,mech}(\phi)$ is in excellent agreement with $G'_{p,EEI}(\phi)$ using a = 459 nm. Thus, $G'_{p,mech}(\phi)$ of this emulsion is highly consistent with past mechanical measurements on other fractionated emulsions that have similar compositions.

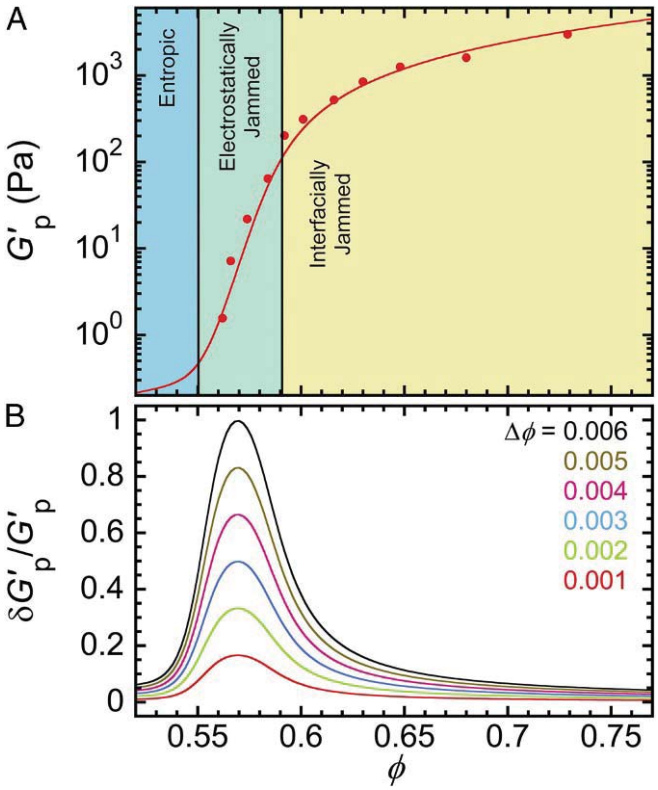

Fig. 1. (*A*) Measured mechanical plateau elastic shear moduli, $G'_{p,mech}(\phi)$, of a monodisperse emulsion having an average droplet radius a = 459 nm (red solid circles). Red solid line: prediction of $G'_{p,EEI}(\phi)$ based on a model of disordered, uniform, concentrated, ionically stabilized droplets that has entropic, electrostatic, and interfacial terms in its free energy [i.e., the EEI model (30); main text]. Regimes in ϕ having different dominant contributions to G'_p in the EEI model are indicated by background colors: entropic (blue), electrostatic (green), and interfacial (yellow). (*B*) Predicted relative uncertainty in G'_p, given by $\delta G'_p/G'_p$, associated with different uncertainties in ϕ given by $\Delta\phi$ (*Upper Right Inset*).

Since the EEI model smoothly captures the steep rise in $G'_p(\phi)$, we use it to demonstrate that even relatively small

experimental uncertainties in ϕ of emulsion samples can lead to very large uncertainties in G'_p at the onset of jamming. We first numerically calculate the first partial derivative of $G'_{p,EEI}$ with respect to ϕ. In Fig. 1*B*, we plot the predicted relative magnitude of the variation in $G'_p(\phi)$, which is proportional to this first partial derivative and also proportional to the magnitude of the uncertainty in the droplet volume fraction, $\Delta\phi$. Even for small $\Delta\phi$ significantly less than 1%, measured values of G'_p near the onset of jamming could exhibit significant scatter and uncertainty of a factor of 2 or more. This highlights the need to control ϕ very carefully in all studies of mechanical properties of jammed emulsions, irrespective of whether these measurements are based on mechanical rheometry or on light scattering. Here, we have controlled ϕ to a high degree and have kept $\Delta\phi$ very low. Moreover, we have ensured a direct comparison between mechanical and light-scattering measurements on exactly the same emulsion at the same set of ϕ values, thereby avoiding the large uncertainties in G'_p highlighted by the peaks in Fig. 1*B*, which adversely affected a prior comparison near and above the jamming point (8).

Diffusing Wave Spectroscopy. To facilitate comparison with mechanical results, we performed DWS studies on the same emulsion at identical ϕ (*Materials and Methods*). The measured, normalized, time-averaged intensity autocorrelation functions, $g_2(t)-1$, for each different ϕ are shown for DWS transmission (Fig. 2*A*) and backscattering (Fig. 2*B*). In these measured $g_2(t)-1$, after initial decays, we observe long-time plateaus over at least several orders of magnitude in t, except at the lowest ϕ. Such plateau behavior indicates that droplets in the emulsion are confined by other surrounding droplets. The magnitudes of these plateaus increase systematically toward unity for larger ϕ, indicating greater droplet confinement. For $\phi \geq 0.574$, transmission $g_2(t)-1$ curves remain above the baseline even for long times extending into the echo regime (*Materials and Methods*). By contrast, for $\phi < 0.574$, $g_2(t)-1$ becomes unresolvable from the baseline at long times; so, plateau behavior, if present, cannot be readily determined using transmission DWS for such low ϕ. To overcome this limitation, we also measure $g_2(t)-1$ using backscattering DWS. We also test several larger ϕ to compare backscattering plateaus with clearly resolved transmission plateaus. For $\phi > 0.616$, the backscattering DWS correlation functions do not decay sufficiently to be readily analyzed. For the two lowest ϕ, $g_2(t)-1$ are similar; this is likely caused by experimental uncertainties when setting ϕ.

Extracting Self-Motion of Dense Probes. From DWS $g_2(t)-1$ we extract the apparent MSDs of probe droplets $\langle \Delta \boldsymbol{r}_a^2(t) \rangle$ using standard procedures (31) (*Materials and Methods*). For passive DWS microrheology using tracer probes at low $\phi \sim 1-2\%$ (6, 12, 19), collective scattering effects are negligible and $\langle \Delta \boldsymbol{r}_a^2(t) \rangle$ reduces to the true $\langle \Delta \boldsymbol{r}^2(t) \rangle$ associated with probe self-motion. However, for higher probe concentrations, as in the emulsions here, the individual scattering processes are modulated by the microstructure. In single scattering, this leads to the well-known de Gennes narrowing of the intensity-spectrum $I(q,\omega)$, where q is the magnitude of the scattering wavevector and ω is the frequency of quasi-elastically scattered coherent radiation, near the peak of the structure factor of simple liquids (32). The experimental collective diffusion coefficient of colloids $D_c \propto 1/S(0)$ measured by dynamic light scattering increases with concentration, where the structure factor at low q $S(0)$ drops sharply (32–34). In DWS, collective scattering effects contribute at all scattering wavevectors; consequently, to obtain the self-motion MSD of probes, it is necessary to correct the apparent MSD by multiplying it with the average structure factor $\langle S(q) \rangle$ of the emulsion: $\langle \Delta \boldsymbol{r}^2(t) \rangle = \langle S(q) \rangle \langle \Delta \boldsymbol{r}_a^2(t) \rangle$. $\langle S(q) \rangle$ is defined by the integral of

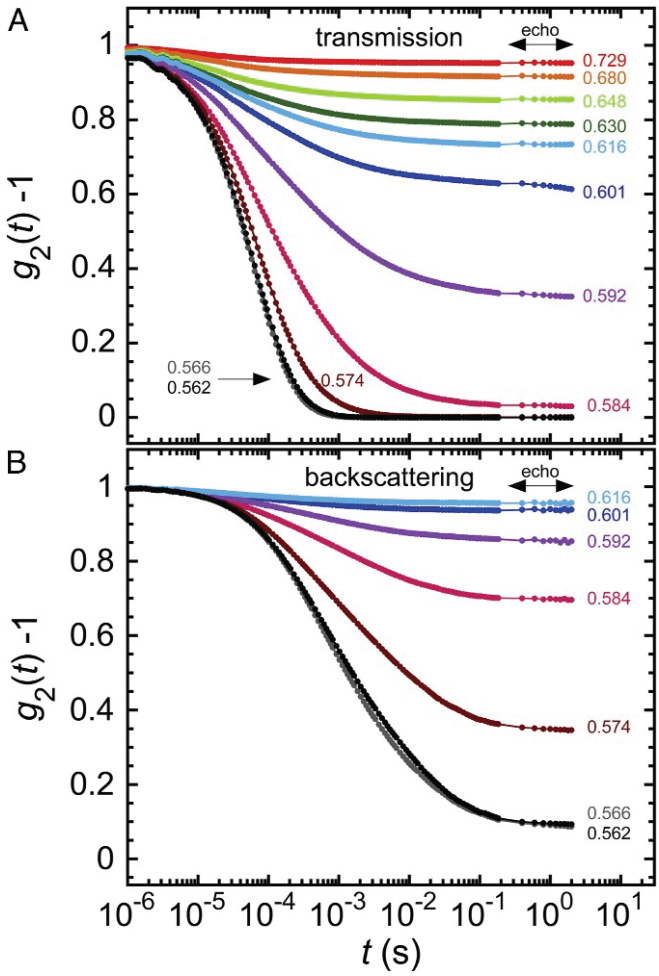

Fig. 2. (*A* and *B*) Normalized, averaged temporal DWS intensity correlation functions, $g_2(t)-1$, of a monodisperse emulsion having a = 459 nm for the same set of ϕ (values on right) as in Fig. 1*A* measured using (*A*) transmission and (*B*) backscattering (*Materials and Methods*). DWS echo data are indicated by arrows. Lines guide the eye.

$S(q)$, over all $q \in [0, 2k]$, weighted by the scattering power $P(q)$ and normalizing: $\langle S(q) \rangle = \int_0^{2k} q^3 P(q) S(q) dq \Big/ \int_0^{2k} q^3 P(q) dq$, where $P(q)$ denotes the form factor of the scatterers and $k = 2\pi n_s/\lambda_{DWS}$ is the wavenumber in the solvent with refractive index $n_s = 1.33$ for water (31, 35). By comparison, a possible contribution by the distinct part of the hydrodynamic function is small, so we neglect it (*SI Appendix*).

To quantify $\langle S(q) \rangle$, we measure $1/\ell^*(\phi)$ for the emulsion with a = 459 nm over a wide range of ϕ by comparing time-averaged transmission intensities from these emulsions with transmission intensities measured for a set of polystyrene latex reference samples having different sizes, using the DWS instrument's software (5) (Fig. 3*A*). Collective scattering also influences static light scattering and thus ℓ^*. Typically, this leads to an increase of ℓ^*, although in some particular cases it can also lead a reduction, e.g., close to a photonic pseudogap or for high refractive index scatterers (36, 37). In Fig. 3*A* we plot the calculated $1/\ell^*_{ISA} \propto \phi$ (dashed line) in the absence of collective scattering, also known as the independent scattering approximation (ISA). Using $n_s = 1.33$ for water, we infer that the refractive index of the oil inside the droplets is $n = 1.401$ using the criterion that $1/\ell^*_{ISA}$ and $1/\ell^*$ must merge as $\phi \to 0$. This oil refractive index is in excellent agreement with refractometry measurements that we have made ($n = 1.40$ at $\lambda \sim 580$ nm) and also the supplier's reference

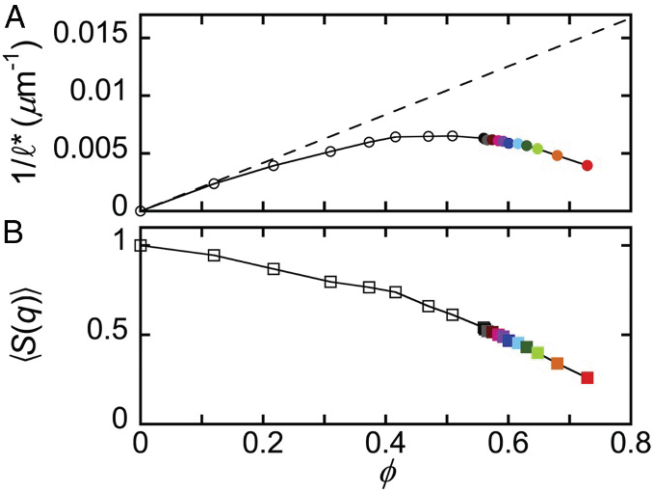

Fig. 3. (*A*) Measured inverse mean free path of optical transport, $1/\ell^*$ (circles), for a monodisperse emulsion having a = 459 nm as a function of ϕ. Colored solid circles encode ϕ of elastically jammed droplets (Fig. 2). Solid line guides the eye. Straight dashed line corresponds to the ISA (main text) and approaches the measured $1/\ell^*$ at low ϕ. (*B*) Measured average ϕ-dependent structure factor $\langle S(q)\rangle$ (squares) determined by dividing $1/\ell^*$ by the extrapolated dashed line $1/\ell^*_{\mathrm{ISA}}$ in *A*. Line guides the eye. Solid squares are color coded as in *A*.

data ($n = 1.403$). Knowing ℓ^*_{ISA}, we determine $\langle S(q)\rangle$ directly by taking advantage of a local collective scattering approximation (CSA) for spherical scatterers: $\langle S(q)\rangle = \ell^*_{\mathrm{ISA}}/\ell^*$ (35) (Fig. 3*B*). Interestingly, $\langle S(q)\rangle$ is reduced by nearly a factor of 4 at the highest ϕ we explore. Thus, accounting for collective scattering necessitates substantial ϕ-dependent corrections to DWS MSDs in concentrated probe systems, as we have demonstrated for concentrated emulsions.

DWS-GSER Microrheology. At each ϕ, we use ℓ^* and details of the scattering geometries to extract apparent MSDs $\langle \Delta \boldsymbol{r}^2_{\mathrm{a}}(t)\rangle$ from DWS $g_2(t) - 1$. We then correct this result using the empirically determined $\langle S(q)\rangle$, yielding $\langle \Delta \boldsymbol{r}^2(t)\rangle$ corresponding to true droplet self-motion. DWS transmission results are shown in Fig. 4*A*. The measured MSDs increase nearly linearly at short times ($t \lesssim 10^{-5}$ s), gradually bend, and saturate to plateau values at long times ($t \gtrsim 10^{-1}$ s). The transmission MSDs for $\phi = 0.562$ and 0.566 have been truncated at longer times because $g_2(t) - 1$ becomes indistinguishable from the baseline there. For lower ϕ, backscattering DWS $g_2(t) - 1$ [cross-polarized detection, denoted VH (5)] provides a more reliable result for $\langle \Delta \boldsymbol{r}^2(t)\rangle$ (Fig. 4*B*). To obtain $\langle \Delta \boldsymbol{r}^2(t)\rangle$ from backscattering DWS for the emulsions, we use a factor of $\gamma_{\mathrm{VH}} = 1.95$ that has been previously found by matching transmission DWS with backscattering DWS for an independent reference sample of polystyrene spheres (*Materials and Methods*). Backscattering MSDs have nearly the same shapes and long-time plateau values as transmission MSDs, yet backscattering MSDs at early times are noisier because light paths are shorter overall and there is less averaging than in transmission. As ϕ is raised, the long-time plateau MSDs $\langle \Delta \boldsymbol{r}^2\rangle_{\mathrm{p}}$ decrease, indicating higher droplet confinement.

We analyze these droplet self-motion MSDs by developing a time-domain fitting function that accounts for the gradual bend in the shape of the dense emulsion MSDs, in addition to the short-time linear rise associated with a high-frequency viscosity η_∞ and a long-time G'_{p}. This gradual bend for dense emulsion systems can be attributed to an $s^{1/2}$ contribution to the frequency-dependent viscoelastic modulus in the Laplace frequency s domain (8, 38). Using the GSER, separating terms in the Laplace domain, and the analytical inverse Laplace transform, we obtain an appropriate time-domain fitting function for measured MSDs in *SI Appendix*, Eq. **S11**, which involves the complementary error function (*Materials and Methods*). Using this equation, which has three fitting parameters, η_∞, $G'_{\mathrm{p,GSER}}$, and a time scale τ associated with the $s^{1/2}$ power law, we least-squares fit both transmission and backscattering MSDs (lines in Fig. 4 *A* and *B*). For all ϕ, we find excellent agreement between the fits and measured MSDs. In addition, because the MSDs are proportional to the linear viscoelastic shear creep compliance, $J(t)$ (7), we directly report the measured and fitted $J(t)$ (Fig. 4, right axes; *Materials and Methods*). For large enough ϕ beyond which short-time noise does not adversely influence the MSDs, we find that $\eta_\infty(\phi)$ rises toward larger ϕ (*SI Appendix*, Fig. S2). We find also that $\tau(\phi)$ decreases strongly as droplets jam toward larger ϕ (Fig. 5*A*). In addition, by plotting $G'_{\mathrm{p,GSER}}$ vs. τ (Fig. 5*B*), we find that an empirical power-law relationship $G'_{\mathrm{p,GSER}} \sim \tau^{-\chi}$, where $\chi = 0.86 \pm 0.02$, holds through the jamming regime over many orders of magnitude in both $G'_{\mathrm{p,GSER}}$ and τ. Thus, the low-frequency plateau viscoelastic moduli of jammed emulsions appear to be correlated in a nontrivial manner to the time scales associated with the higher-frequency $s^{1/2}$ viscoelastic response.

Comparison: DWS-GSER and Mechanical Plateau Moduli. In Fig. 6, we plot the microrheological $G'_{\mathrm{p,GSER}}(\phi)$ obtained as fit parameters to DWS self-motion MSDs and compare these directly to the

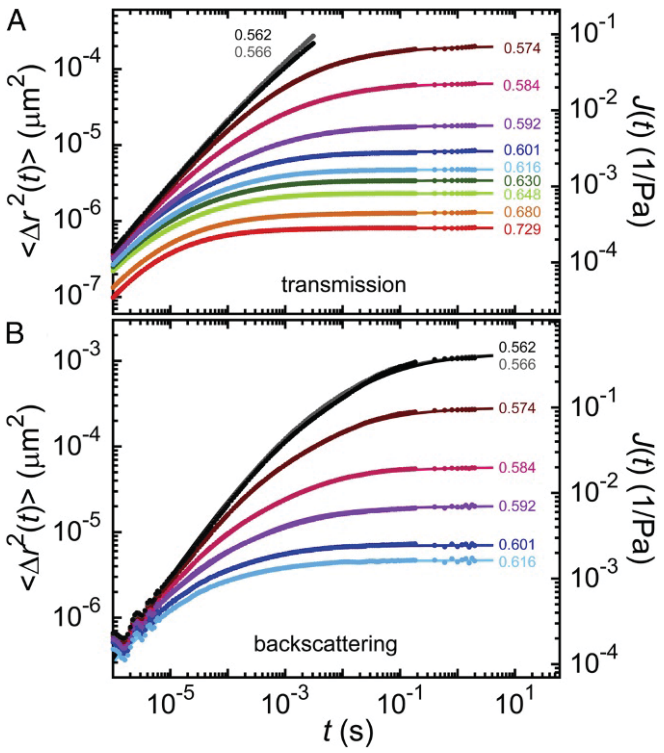

Fig. 4. (*A* and *B*) Ensemble-averaged temporal mean-square displacements, $\langle \Delta \boldsymbol{r}^2(t)\rangle$, corresponding to droplet self-motion in a jammed monodisperse emulsion extracted from $g_2(t) - 1$ (Fig. 2) using $1/\ell^*$ values (Fig. 3*A*) after correcting with ϕ-dependent $\langle S(q)\rangle$ (Fig. 3*B*). (*A*) Transmission DWS. (*B*) Backscattering DWS. Solid lines are least-squares fits to an emulsion MSD model in *SI Appendix*, Eq. **S11** (see also main text); labels for each ϕ are color coded as in Fig. 2. Right axes show shear creep compliance $J(t) \sim \langle \Delta \boldsymbol{r}^2(t)\rangle$ obtained via passive microrheology using the GSER. In *A*, we display only the portions of the transmission MSDs for ϕ = 0.562 and 0.566 that can be reliably extracted above the baseline of $g_2(t) - 1$.

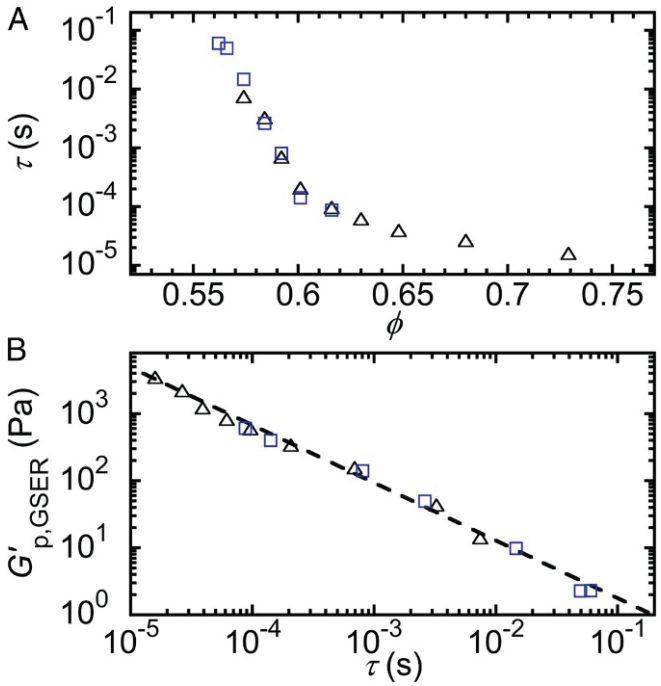

Fig. 5. (*A*) Characteristic time scale τ of the $(s\tau)^{1/2}$ term in the viscoelastic emulsion model (*SI Appendix*), obtained from fits to DWS MSDs in Fig. 4, as a function of ϕ: transmission (open black triangles), and backscattering (open blue squares). (*B*) Plateau elastic storage modulus $G'_{p,GSER}$ as a function of τ, both obtained as fit parameters of DWS MSDs in Fig. 4. Symbols are as in *A*. Dashed line: fit using a power law, $G'_{p,GSER} \sim \tau^{-\chi}$, yielding an exponent $\chi = 0.86 \pm 0.02$.

macroscopic mechanical $G'_{p,mech}(\phi)$ and the predicted $G'_{p,EEI}(\phi)$ of the EEI model. Over the entire range of ϕ, we find excellent agreement between DWS microrheological and mechanical G'_p measurements without applying any arbitrary correction factors, which had been previously applied to dense emulsion systems on an ad hoc and ϕ-independent basis (8, 29). Accounting for collective scattering effects in DWS MSDs by using ϕ-dependent $\langle S(q)\rangle$, based on the measured $\ell^*(\phi)$, is necessary to achieve such quantitative agreement.

Conclusions

Since the advent of passive microrheology, apparent DWS MSDs have been used in combination with the GSER to show trends in $G'_p(\phi)$ of dense glassy and jammed colloidal systems, including emulsions, yet until now a highly accurate quantitative match with macroscopic mechanical measurements has not been obtained over a wide range of ϕ. In past experiments, the lack of conversion of apparent MSDs into true self-motion MSDs has led to the introduction of various correction factors to rescale microrheological measurements into mechanical measurements as well as theoretical speculations about appropriateness of boundary conditions and other assumptions inherent in the GSER. Here, we have shown that invoking such ad hoc correction factors is unnecessary, and we have presented and demonstrated a well-defined empirical method for correcting DWS MSDs in dense, highly scattering systems using ϕ-dependent $\langle S(q)\rangle$ to account for collective scattering. Although the q^3 weighting inherent in DWS does favor self-motion in the extracted MSDs, such extracted MSDs still require significant ϕ-dependent corrections for scattering probes at high densities, up to a factor of 4 or more, as we have demonstrated for jammed emulsions. The excellent agreement we find between $G'_p(\phi)$ measured using both modern DWS-GSER microrheology and mechanical rheometry implies that the GSER does work very well for dense emulsion systems if the DWS MSDs have been properly corrected for collective scattering. In addition, the microrheological $G'_p(\phi)$ matches the predicted $G'_p(\phi)$ of the EEI model as droplets become jammed, which enables us to identify that the GSER is applicable when both screened electrostatic repulsions and droplet interfacial deformations dominate $G'_p(\phi)$. Moreover, we have derived a time-domain equation for MSDs of droplets in dense emulsions, based on the GSER and a model that has an $s^{1/2}$-dependent contribution to the linear viscoelasticity, and have used this equation to fit measured DWS self-motion MSDs, yielding excellent agreement. From these fits, we have determined the ϕ-dependent time scale τ associated with the $s^{1/2}$ term in the viscoelastic model. In future theoretical investigations, it would be useful to determine quantitative predictions for $\tau(\phi)$ and the power-law scaling identified for $G'_p(\tau)$ that could be compared with our measurements. We anticipate that broader application of the method we have demonstrated for correcting DWS MSDs of jammed emulsions with the ϕ-dependent $\langle S(q)\rangle$ could lead to improved quantitative accuracy of passive microrheology using the GSER in other dense colloidal soft materials that are highly scattering.

Materials and Methods

Monodisperse Oil-in-Water Emulsions. We make emulsions using SDS (Fisher Scientific; electrophoresis grade 99% purity), PDMS (Gelest Inc.; viscosity 350 centi-Stokes), and deionized water (Millipore Milli-Q; resistivity 18.2 MΩ·cm). SDS-stabilized monodisperse PDMS O/W emulsions were prepared through emulsification, a set of depletion fractionation steps to reduce droplet polydispersity (39), and repeated centrifugation to set the bulk concentration of SDS and to concentrate the droplets (40–43) (*SI Appendix*). Samples at lower ϕ were prepared by diluting the concentrated master emulsion sample with 10 mM SDS solution. The master emulsion is also diluted in 10 mM SDS to $\phi \sim 10^{-4}$ and then characterized by multiangle DLS (LS Spectrometer; LS Instruments) over $60^\circ - 120^\circ$ scattering angles, yielding an average hydrodynamic droplet radius $a = 459 \pm 15$ nm. The polydispersity is $\delta a/a \simeq 0.176$, where δa is the SD of the radial droplet size distribution.

Mechanical Shear Rheometry. For each ϕ, we load the emulsion sample into a 25-mm diameter stainless steel cone-and-plate geometry in a

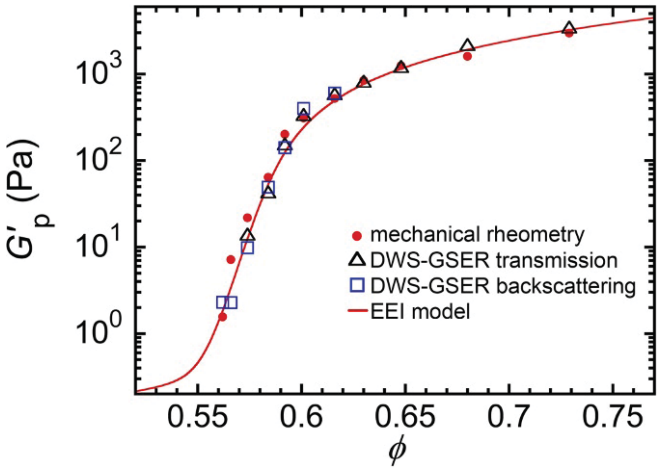

Fig. 6. Comparison of plateau shear elastic moduli G'_p of a monodisperse emulsion as a function of ϕ as disordered droplets jam. $G'_{p,mech}(\phi)$ was measured using mechanical shear rheometry (solid red circles) (Fig. 1). $G'_{p,GSER}(\phi)$ was measured using the $\langle S(q)\rangle$-corrected plateau DWS MSDs at long times t in Fig. 4 through the GSER of passive microrheology: transmission (open black triangles) and backscattering (open blue squares). Red solid line shows $G'_{p,EEI}(\phi)$ predicted by the EEI model.

strain-controlled shear rheometer (Rheometrics RFS-II, equipped with a vapor trap). For a low strain in the linear regime, we measure frequency sweeps to obtain the low-frequency plateau $G'_{p,mech}(\phi)$ (*SI Appendix* and *SI Appendix*, Fig. S1).

DWS. We perform DWS measurements (DWS RheoLab III; LS Instruments) to obtain the intensity correlation functions for emulsions at different ϕ. Each emulsion sample is loaded into an $L = 5$-mm path-length glass cuvette. After the initial loading, each cuvette is very gently centrifuged to remove the air bubbles without creating gradients in ϕ; after removing air bubbles, each emulsion is then allowed to equilibrate for 1 d before any DWS measurements are performed. At all times, the temperature is controlled and maintained at $T = 20^\circ \pm 0.1^\circ$C. A coherent light source (wavelength $\lambda_{DWS} = 687$ nm) is directed to the surface of a rotating ground-glass diffuser so that the speckle beam from the rotating glass diffuser can provide an efficient ensemble-averaged signal from the recorded correlation echoes (27). The scattered light is collected in a transmission or in a backscattering geometry to obtain normalized intensity autocorrelation function $g_2(t)$ in the homodyne limit. A total of 5–10 runs of 300 s were performed and averaged for each emulsion sample (4). DWS echo data are also acquired at longer times. From the measured $g_2(t)$ and ℓ^*, we extract the apparent $\left\langle \Delta \boldsymbol{r}_a^2(t) \right\rangle$ and, using the CSA approximation and measured $\ell^*(\phi)$, we determine true droplet self-motion $\left\langle \Delta \boldsymbol{r}^2(t) \right\rangle$ (*SI Appendix*).

Fitting Droplet Self-Motion MSDs to Extract Rheological Parameters. We fitted the measured droplet self-motion MSDs to an analytical time-domain equation (*SI Appendix*, Eq. **S11**) based on the generalized Stokes–Einstein relation and a model for linear viscoelasticity of emulsions that includes a low-frequency plateau shear modulus G'_p, a high-frequency viscosity η_∞, and an $s^{1/2}$ high-frequency viscoelastic contribution with a characteristic time constant τ (8, 38): $\tilde{G}(s) = G'_p[1 + (s\tau)^{1/2}] + \eta_\infty s$. This model may also be appropriate for concentrated hard spheres in a viscous liquid (44, 45).

ACKNOWLEDGMENTS. H.S.K. and T.G.M. thank the University of California, Los Angeles for financial support. N.S., C.Z., and F.S. acknowledge funding by the Swiss National Science Foundation through Project 169074 and the National Center of Competence in Research Bio-Inspired Materials. F.S. acknowledges financial support by the Adolphe Merkle Foundation.

1. Maret G, Wolf PE (1987) Multiple light scattering from disordered media. The effect of Brownian motion of scatterers. *Z Phys B* 65:409–413.
2. Pine DJ, Weitz DA, Chaikin PM, Herbolzheimer E (1988) Diffusing wave spectroscopy. *Phys Rev Lett* 60:1134–1137.
3. Weitz D, Pine D, Pusey P, Tough R (1989) Nondiffusive Brownian motion studied by diffusing-wave spectroscopy. *Phys Rev Lett* 63:1747–1750.
4. Scheffold F, Schurtenberger P (2003) Light scattering probes of viscoelastic fluids and solids. *Soft Matter* 1:139–165.
5. Zhang C, Reufer M, Gaudino D, Scheffold F (2017) Improved diffusing wave spectroscopy based on the automatized determination of the optical transport and absorption mean free path. *Korea-Aust Rheol J* 29:241–247.
6. Mason TG, Weitz DA (1995) Optical measurements of frequency-dependent linear viscoelastic moduli of complex fluids. *Phys Rev Lett* 74:1250–1253.
7. Squires TM, Mason TG (2010) Fluid mechanics of microrheology. *Annu Rev Fluid Mech* 42:413–438.
8. Mason TG, Gang H, Weitz D (1997) Diffusing-wave-spectroscopy measurements of viscoelasticity of complex fluids. *J Opt Soc Am A* 14:139–149.
9. Dasgupta BR, Tee SY, Crocker JC, Frisken BJ, Weitz DA (2002) Microrheology of polyethylene oxide using diffusing wave spectroscopy and single scattering. *Phys Rev E* 65:051505.
10. Hemar Y, Pinder DN (2006) DWS microrheology of a linear polysaccharide. *Biomacromolecules* 7:674–676.
11. Oelschlaeger C, Cota Pinto Coelho M, Willenbacher N (2013) Chain flexibility and dynamics of polysaccharide hyaluronan in entangled solutions. *Biomacromolecules* 14:3689–3696.
12. Mason TG, Ganesan K, van Zanten JH, Wirtz D, Kuo SC (1997) Particle tracking microrheology of complex fluids. *Phys Rev Lett* 79:3282–3285.
13. Mason TG, Dhople A, Wirtz D (1997) Concentrated DNA rheology and microrheology. *MRS Proc Stat Mech Phys Biol* 463:153–158.
14. Xing Z, et al. (2018) Microrheology of DNA hydrogels. *Proc Natl Acad Sci USA* 115:8137–8142.
15. Palmer A, Mason TG, Xu J, Kuo SC, Wirtz D (1999) Diffusing wave spectroscopy microrheology of actin filament networks. *Biophys J* 76:1063–1071.
16. Gisler T, Weitz DA (1999) Scaling of the microrheology of semidilute F-actin solutions. *Phys Rev Lett* 82:1606–1609.
17. Mason TG, Gisler T, Kroy K, Frey E, Weitz DA (2000) Rheology of F-actin solutions determined from thermally driven tracer motion. *J Rheol* 44:917–928.
18. Scheffold F, et al. (2010) Brushlike interactions between thermoresponsive microgel particles. *Phys Rev Lett* 104:128304.
19. Willenbacher N, et al. (2007) Broad bandwidth optical and mechanical rheometry of wormlike micelle solutions. *Phys Rev Lett* 99:068302.
20. Cardinaux F, Cipelletti L, Scheffold F, Schurtenberger P (2002) Microrheology of giant-micelle solutions. *Europhys Lett* 57:738–744.
21. Oelschlaeger C, Schopferer M, Scheffold F, Willenbacher N (2009) Linear-to-branched micelles transition: A rheometry and diffusing wave spectroscopy (DWS) study. *Langmuir* 25:716–723.
22. Xue JZ, Pine DJ, Milner ST, Wu XI, Chaikin PM (1992) Nonergodicity and light scattering from polymer gels. *Phys Rev A* 46:6550–6563.
23. Romer S, Scheffold F, Schurtenberger P (2000) Sol-gel transition of concentrated colloidal suspensions. *Phys Rev Lett* 85:4980–4983.
24. Scheffold F, Skipetrov S, Romer S, Schurtenberger P (2001) Diffusing-wave spectroscopy of nonergodic media. *Phys Rev E* 63:061404.
25. Viasnoff V, Lequeux F, Pine D (2002) Multispeckle diffusing-wave spectroscopy: A tool to study slow relaxation and time-dependent dynamics. *Rev Sci Instrum* 73:2336–2344.
26. Schurtenberger P, et al. (2003) Aggregation and gelation in colloidal suspensions: Time-resolved light and neutron scattering experiments. *Mesoscale Phenomena in Fluid Systems*, eds Case F, Alexandridis P (Am Chemical Soc, Washington, DC), Vol 861, pp 143–160.
27. Zakharov P, Cardinaux F, Scheffold F (2006) Multispeckle diffusing-wave spectroscopy with a single-mode detection scheme. *Phys Rev E* 73:011413.
28. Gang H, Krall AH, Weitz DA (1995) Thermal fluctuations of the shapes of droplets in dense and compressed emulsions. *Phys Rev E* 52:6289–6302.
29. Braibanti M, et al. (2017) The liquid-glass-jamming transition in disordered ionic nanoemulsions. *Sci Rep* 7:13879.
30. Kim HS, Scheffold F, Mason TG (2016) Entropic, electrostatic, and interfacial regimes in concentrated disordered ionic emulsions. *Rheol Acta* 55:683–697.
31. Qiu X, et al. (1990) Hydrodynamic interactions in concentrated suspensions. *Phys Rev Lett* 65:516–519.
32. Hansen J, McDonald I (2013) *Theory of Simple Liquids* (Academic, Oxford), 4th Ed.
33. Ladd AJC, Gang H, Zhu JX, Weitz DA (1995) Time-dependent collective diffusion of colloidal particles. *Phys Rev Lett* 74:318–321.
34. Nägele G (1996) On the dynamics and structure of charge-stabilized suspensions. *Phys Rep* 272:215–372.
35. Fraden S, Maret G (1990) Multiple light scattering from concentrated, interacting suspensions. *Phys Rev Lett* 65:512–515.
36. Rojas-Ochoa LF, Mendez-Alcaraz J, Sáenz J, Schurtenberger P, Scheffold F (2004) Photonic properties of strongly correlated colloidal liquids. *Phys Rev Lett* 93:073903.
37. Gómez-Medina R, et al. (2012) Negative scattering asymmetry parameter for dipolar particles: Unusual reduction of the transport mean free path and radiation pressure. *Phys Rev A* 85:035802.
38. Liu AJ, Ramaswamy S, Mason TG, Gang H, Weitz DA (1996) Anomalous viscous loss in emulsions. *Phys Rev Lett* 76:3017–3020.
39. Bibette J (1991) Depletion interactions and fractionated crystallization for polydisperse emulsion purification. *J Colloid Interf Sci* 147:474–478.
40. Mason TG, Bibette J, Weitz DA (1995) Elasticity of compressed emulsions. *Phys Rev Lett* 75:2051–2054.
41. Mason TG, et al. (1997) Osmotic pressure and viscoelastic shear moduli of concentrated emulsions. *Phys Rev E* 56:3150–3166.
42. Mason TG, Krall AH, Gang H, Bibette J, Weitz DA (1996) *Monodisperse Emulsions: Properties and Uses*, ed Becher P (Marcel Dekker, New York), Vol 4, pp 299–336.
43. Zhu X, Fryd MM, Huang JR, Mason TG (2012) Optically probing nanoemulsion compositions. *Phys Chem Chem Phys* 14:2455–2461.
44. Rojas L, et al. (2003) Particle dynamics in concentrated colloidal suspensions. *Faraday Discuss* 123:385–400.
45. Lionberger RA, Russel WB (1994) High frequency modulus of hard sphere colloids. *J Rheol* 38:1885–1908.